



Esra Türen  · Hakan Yavuz

# Schlieren imaging investigation of flow fields in synthetic jets generated by different orifice geometries with varying aspect ratios

Received: 15 October 2022 / Revised: 9 January 2023 / Accepted: 7 March 2023 / Published online: 30 March 2023  
© The Visualization Society of Japan 2023

**Abstract** The presented experimental study is based on flow fields investigation of jet structure formations. The studied jet structures are generated by various orifice geometries by an impinging synthetic jet actuator. The characteristic of the generated jet is studied for a range actuator excitation-related electrical parameters. The synthetic jet actuator is driven using varying electrical excitation frequencies, such as 4, 6 and 8 Hz and varying excitation voltage amplitudes such as 1, 1.5 and 2 V. The waveform of the electrical signal is only chosen to be a square wave. In addition to the electrical properties of the excitation signal, a comprehensive examination of characteristics of the synthetic jets generated by different orifice geometries such as circular, rectangular and sinusoidal types is also studied. For determination of the characteristics of the synthetic jets generated, the experimental results are then examined for the electrical excitation related parameters as well as the orifice geometry related properties. It is observed that the geometry of the orifice structure and the electrical parameters of the excitation signal play an important role in determination of the flow properties and performance of the synthetic jets. The achieved results indicate that there is a considerable potential for industrial applications in areas such as electronic device cooling, heat transfer in optical applications, jet structure formation, oscillating flow generation and mixing flow.

**Keywords** Synthetic jet · Orifice · Flow visualization · Schlieren imaging

## 1 Introduction

The synthetic jet mechanism has a long history dating back to the 1950s. Ingard and Labate (1950) performed the first research on acoustic streaming. Dauphinee (1957) designed and studied the first successful synthetic jet actuator using a diaphragm air jet system in the laboratory. Lighthill (1978) observed the flow known as acoustic flow. In the late twentieth century, studies in this area have expanded. Smith and Glezer (1998) made a comprehensive study on synthetic jets and introduced the term “Synthetic Jet” to the literature. Since the beginning of the twenty-first century, many numerical and experimental studies have been carried out on the structures of synthetic jets (Cater and Soria 2002; Chaudhry and Zhong 2014; Trávníček 2015).

In recent years, the topic of synthetic jets has attracted the attention of many researchers. The main reason for such a popularity is the wide range of application areas such as mixing vessels (Xia et al. 2013), heat transfer applications (Youmin et al. 2014; Tesař and Trávníček 2005), cooling of electronic devices

---

E. Türen (✉) · H. Yavuz  
Mech. Eng. Department, Çukurova University Engineering Faculty, Sarıcam, Adana, Turkey  
E-mail: essraturen@gmail.com

H. Yavuz  
E-mail: hyavuz@cu.edu.tr

(Chaudhari et al. 2010; Broučková and Trávníček 2014) and flow separation control of aircraft wings (Gillarranz et al. 2005; Farnsworth et al. 2008; Mohseni 2004; Yang et al. 2022). The main principle of a synthetic jet mechanism is to create an impinging jet flow. The impinging jet flow is generated by back and forth motion of the air achieved as a result of actuator membrane oscillation. During upper motion of the actuator membrane oscillations, a synthetic jet flow above the orifice surface is generated (Didden 1979). Then, during the downward motion of the actuator membrane oscillation, the injected air is sucked back downwards towards the orifice. This cycle is repeated with the above-mentioned stages.

There are three main properties of the actuators and related structures that affect the formation of the synthetic jets, namely as electrical, fluidic and geometric (Murugan et al. 2016). It is also worth noting that the actuator selection is an important parameter for the generation of the synthetic jet. There are some popular actuator types such as piston-cylinder (Duan and Wang 2015), piezoelectric (Yang et al. 2009 and Goodfellow, 2013) and loudspeaker (Trávníček 2015 and Broučková, 2019). They are mainly based on diaphragm movement in generating the synthetic jet. Mallinson et al. (2004) examined a piezoelectric diaphragm and a loudspeaker that was created using the piston-cylinder mechanism as a moving surface. It was reported that the frequency and amplitude characteristics of the actuators of the piston-cylinder, loudspeaker and piezoelectric diaphragm types generally differ from each other. In the piston-cylinder mechanism, the frequency is low, but the amplitude is larger. In piezoelectric diaphragms, the frequency is high, but the amplitude is very low. In the speaker system, the frequency and amplitude are at medium levels compared to other two systems. Wang et al. (2010) experimentally investigated a new signal wave pattern by changing the absorption duty cycle in a two-dimensional synthetic jet mechanism. It has been observed that the distributions of the mean and turbulent flow fields for synthetic jets produced at different suction duty cycle values have properties similar to those shown for the conventional synthetic jet.

The use of speaker in the synthetic jet applications is preferred due to its fast response time and its ability to integrate into other system easily. A change in the diaphragm cavity in the synthetic jet mechanism affects the jet structure formed in the orifice. Feero et al. (2015) examined the performance of cylindrical, conical and curvilinear contraction structures in the cavity structure of the diaphragm. It has been noted that the cavity oscillation has the highest efficiency in the oscillation in the curvilinear tapering structure. Another feature that affects the jet structure of the synthetic jet is varying the electrical parameters of the actuator. Zhang et al. (2015) investigated the synthetic jet mechanism numerically. They reported that the heat transfer performance is increased with the increase in frequency of the electrical signal. Jeng et al. (2016) studied the effects of the diaphragm geometry on the jet structure by varying the electrical parameters of synthetic jet actuators. Another feature that affects the jet structure formed in the synthetic jet is the geometric parameters such as orifice diameter, orifice thickness, cavity diameter and cavity height. Also, the formation of the synthetic jet in different geometries also leads to different formation of the jet structure. Fanning et al. (2015) used a loudspeaker system in the synthetic jet actuator mechanism and the rectangular jet exit geometry. Significant interaction between adjacent synthetic jets was observed in the rectangular slot design. Kim et al. (2010) investigated two types of synthetic jet geometry (rectangular and circular) both experimentally and numerically. In their experiments, it was observed that the velocity reduction tendencies of the synthetic jets were different along the jet stream distance depending on the orifice configuration and the excitation frequency. Oren et al. (2009) reported the changes in flow properties of circular and non-circular orifice configurations (slit, square, equilateral triangle). Configurations were compared with PIV images. It was reported that circular and square configurations were more suitable structures for the purposes of the present study.

Zhang and Zhong (2009) experimented flow control in water by creating an array of circular synthetic jet structures on a wing. The flow visualization was performed with laser-induced fluorescence. The flow separation delay has been observed to be associated with the presence of two or three lines of high flow rate lines in the separated flow. As a result, two contour maps were created based on the flow structure and the effectiveness of the release control under different actuator operating conditions.

Flow visualizations are used to better observe and examine the jet structure formed in the synthetic jet actuator mechanism. Schlieren flow visualization technique is one of the flow visualization methods used to observe synthetic jet structures. Smith and Glezer (1998) investigated a synthetic jet structure in rectangular slot configuration. Schlieren flow visualization and velocity measurements were examined for synthetic jet flow structure. The 2D study results were compared with the traditional synthetic jet structure. As a result, it was observed that the traditional synthetic jet receives more fluid from the environment and loses momentum faster than that of the synthetic jet structures.

Smith and Swift (2001) generated different synthetic jet structures using four nozzles varying according to four design factors. The effects of stroke length and driving frequency values on the formation of synthetic jet structures were investigated with Schlieren flow visualization technique. As a result, it has been observed that it has smaller movement with large stroke length compared to Reynolds number jets with small stroke length. Schlieren flow visualization was used to examine the plasma synthetic jet structures. Zong and Kotsanis (2017) performed experiments on the plasma synthetic jet actuator in two different structures as orifice and slot. It was investigated by PIV measurements and Schlieren flow visualization. The slot jet has a higher drag velocity of the surrounding air than the orifice jet structure. As a result, it is observed that the jet flow results in a lower spread velocity. Dang et al. (2015) examined Schlieren flow visualization in dual synthetic jet structures. The vector angle can be adjusted by controlling the movement of the dual synthetic jet's control performance moving. It was also seen that the dual synthetic jet structure can effectively reduce the errors caused by the instability of the flow field.

Another method used for flow visualization is the oil visualization technique. Although the oil visualization method is a cheap and effective method, its usage area is quite rare. Ozkan (2016) used the oil flow visualization method on the NACA 4412 airfoil in his study. Genç et al. (2011) investigated the suppression of laminar separation bubbles with the help of oil visualization by blowing and/or suction on the NACA 2415 blade model. In this study, the separation of flow and attachment points on the wing, as well as the effect of tip vortices on the wing, were investigated. Although the oil mixture remained stationary in the separation bubble region, the oil mixture appears to move with the flow in other regions. Feero et al. (2016) used oil visualization to observe reattached flow using a synthetic jet actuator in the NACA 0025 airfoil. In this study, the effect of excitation frequency and blowing ratio with oil visualization was examined. As a result, a similar narrowing of the aperture extension of the flow bound to the trailing edge was observed due to the trailing edge effects of the finite span jet at the excitation frequency. It was also determined that increasing the blowing ratio reduces the amount by which the attached flow contracted.

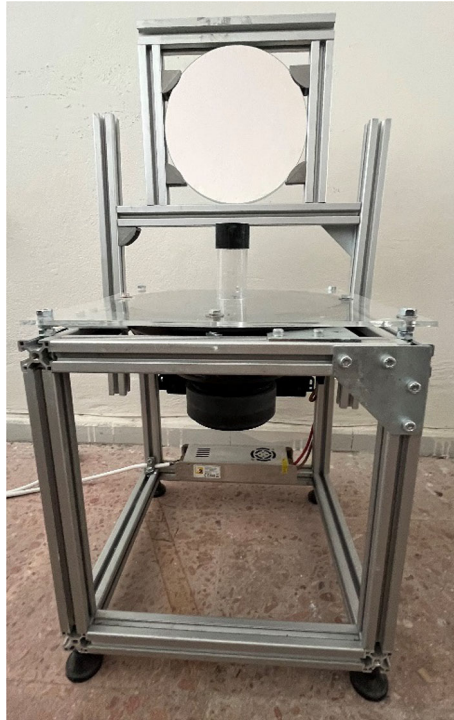
The aim of the study is to examine the synthetic jets structures produced with different orifice geometries such as circular, rectangular and sinusoidal types. The produced jets are generated using the square wave excitation type of signal. To examine the effects on the evolution of synthetic jet structures in terms of orifice structures with different aspect ratios, excitation frequencies (4, 6 and 8 Hz) and excitation voltage amplitudes (1, 1.5 and 2 V), in addition to the changes in orifice geometries, Schlieren and oil visualization techniques are performed to determine the characteristic features of synthetic jets. It is expected that the presented study contributes to the literature as a parametric study of various synthetic jet geometries and their effects on related flow fields. These flow fields can be used in a number of applications mainly where there is a need for improved heat transfer and better cooling effects. The applications can also be extended to mixing flow with improved mixing rate. In addition, the form of flow in enclosure area where the continuous flow is converted to oscillating type to prevent partial blockage and to improve flow rate.

## 2 Experimental setup

A synthetic jet mechanism is constructed, and a loudspeaker is used as an actuator. The synthetic jet mechanism system, designed for this study, is shown in Fig. 1. In order to create an impinging synthetic jet flow in the system, JBL CS-1214 30 cm 1000 W model loudspeaker is used as an actuator. In the synthetic jet actuator mechanism, a power source is connected to drive the loudspeaker. UNI-T UTG-9005C signal generator is used to adjust the excitation frequency and the application voltage in the loudspeaker. A transparent Plexiglas with dimensions of 300 × 300 mm and a thickness of 5 mm, with an orifice cavity in the middle of 30 cm in diameter, is placed on top of the loudspeaker. The sealing is provided between the Plexiglas and the speaker for insulation.

In this study, the excitation frequencies of 4, 6 and 8 Hz and the excitation voltages in the operating range of 1, 1.5 and 2 V are investigated. The application values of the excitation frequency and the applied voltage values along with the different geometric models used are presented in Table 1.

Three different geometric models are chosen to examine the effects of jet structures in different orifice geometries of the synthetic jet mechanism. A circular, rectangular and sinusoidal types are determined as orifice geometric models of the synthetic jet mechanism. In addition to the examinations of cylinder and rectangular jet geometries, additionally a sinusoidal (new geometry) geometric structure is also considered for the study. It is noted that the circular and rectangular orifice outlets are used in the literature. But the sinusoidal geometric structure is a new geometric form. In order to investigate the effect of the sinusoidal



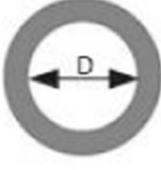
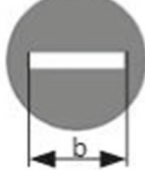

**Fig. 1** Experimental setup of the synthetic jet mechanism

geometric structure, it is compared with the vortex structures formed under the same conditions in circular and rectangular orifice structures used in the literature. In the selection of the sinusoidal jet geometry, it was designed by predicting that it would have a wide impact area and improvements in the formation of synthetic jet. The effects of the sinusoidal jet geometry on different geometric ratios are investigated. The jet structures are very important in the use of synthetic jets to investigate the effect of the parameters on forming of the vortex ring.

As a part of the analysis, the effects of geometric models in 5 different aspect ratios of three different jet models on vortex structures are investigated. In addition, the effects of geometric models in 5 different aspect ratios belonging to three different jet models on eddy structures are investigated. In their study Persons et al. (2011) used the orifice diameter of 5 mm, and Holman et al. (2005). Kim et al. (2010) determined the geometric dimensions of the rectangular orifice as 0.6 mm and the opening as 50 mm. According to these studies, the orifice geometry for the cylinder was determined as 5, 10, 20, 30, 40 mm working parameters in order to examine a wide working range. While creating rectangular and sinusoidal orifice geometries, models with fixed 5 mm thickness and increasing length ratios (5, 10, 20, 30, 40 mm) are created. In this study, the effect of the length change of the models on flow field is examined, which sets the presented study apart from the others in the literature. The details of these geometries and related geometric ratios are shown in Table 2.

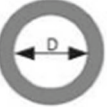

















In order to create different geometric models of the orifice structure of the synthetic jet actuator mechanism, criteria such as length/diameter and thickness ratios are determined. Smit and Glezer (1998) used a rectangular orifice in their study. The rectangular structure was examined by looking at the aspect ratios. Also, Lin (2014) used rectangular structure orifice structure in the synthetic jet actuator. Kumar et al. (2021) investigated the vortex ring bifurcations formed in a rectangular synthetic jet. In this study, the diameter ( $D$ ) is used in the cylindrical orifice structure and assumed as characteristic length in the geometry. Based on these studies, the distance from the beginning and the end of the “S” structure in the sinusoidal orifice structure is accepted as  $b$  distance, since the long side in the rectangular orifice structure is taken as “ $b$ ”. In this study, the dimensions are determined as  $b = D = 40, 30, 20, 10$  and 5 mm. A fixed thickness of 5 mm is determined in the rectangular and sinusoidal orifice geometric models of the synthetic jet actuator. In Table 2, there are models of variation in dimensional ratios of cylindrical, rectangular and sinusoidal models.

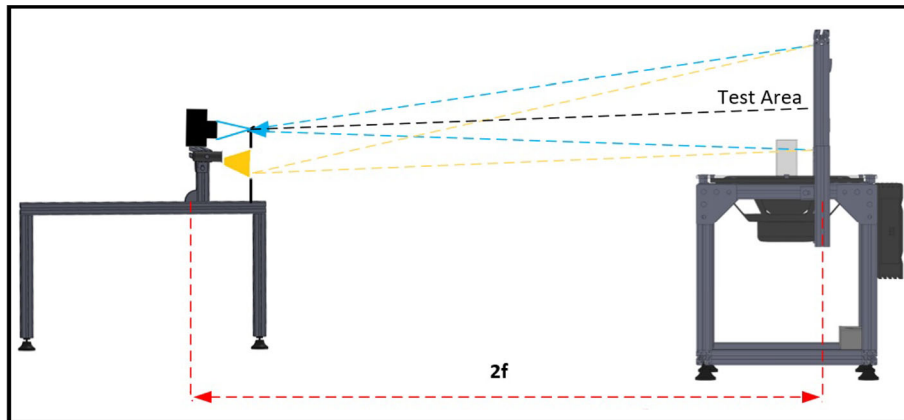
**Table 1** Synthetic jet geometries, excitation frequency and applied voltage values

| Synthetic Jet Name                            | Cylinder  | Rectangular  | Sinusoidal  |
|---|---|--|---|
| Synthetic Jet Geometries                      |  |  |  |
| Synthetic Jet Orifice Dimension (D=b)         | 40 - 5 mm   | 40 - 5 mm  | 40 - 5 mm   |
| Frequency (Hz) And Applied Voltage (V) Values | 4 Hz 1 V  | 4 Hz 1 V   | 4 Hz 1 V  |
|   | 4 Hz 1.5 V  | 4 Hz 1.5 V   | 4 Hz 1.5 V  |
|   | 4 Hz 2 V  | 4 Hz 2 V   | 4 Hz 2 V  |
|   | 6 Hz 1 V  | 6 Hz 1 V   | 6 Hz 1 V  |
|   | 6 Hz 1.5 V  | 6 Hz 1.5 V   | 6 Hz 1.5 V  |
|   | 6 Hz 2 V  | 6 Hz 2 V   | 6 Hz 2 V  |
|   | 8 Hz 1 V  | 8 Hz 1 V   | 8 Hz 1 V  |
|   | 8 Hz 1.5 V  | 8 Hz 1.5 V   | 8 Hz 1.5 V  |
|   | 8 Hz 2 V  | 8 Hz 2 V   | 8 Hz 2 V  |

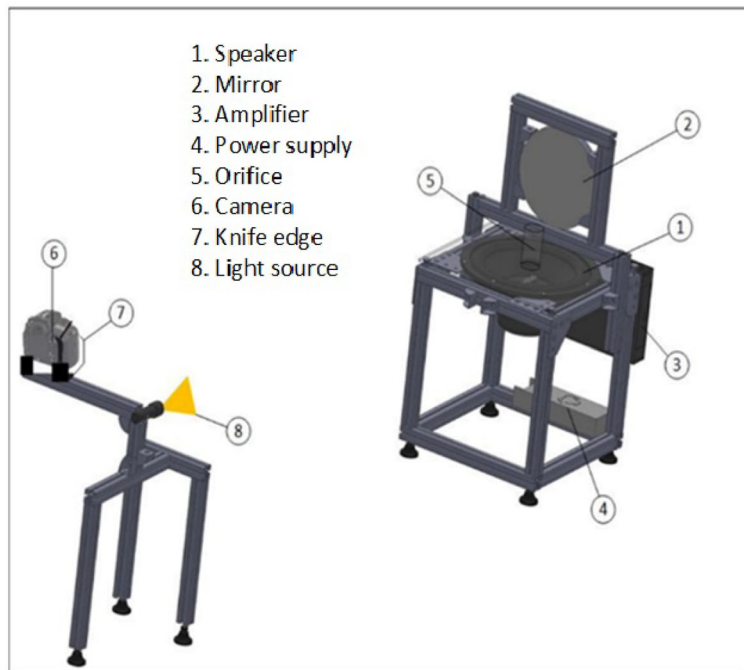
The Schlieren imaging system is used to examine the flow visualization of the designed orifice geometries. The synthetic jet mechanism and Schlieren imaging system are designed using CAD drawing software. The experimental set-up of the system is shown in Fig. 2. A 203-mm-long Schlieren mirror is used in the Schlieren visualization system. The focal diameter of the mirror is about 75 mm ( $f$ ). For this reason, the light source is placed between the mirror and the light at a distance of  $2f = 150$  mm. A knife edge is placed at the focus point where the light distance came from. A camera is placed behind the knife edge to view it. In the Schlieren imaging system, it is very important to set the light and focal length correctly. The formation of the image in the Schlieren system is obtained by the formation of the density difference. For

**Table 2** Geometrical dimensions of the synthetic jet outlet

| Orifice     | Diameter  | Length (D=b)  |   |   |  |   |
|-------------|---|---|---|---|--|---|
|             |   | 40 mm   | 30 mm   | 20 mm   | 10 mm  | 5 mm  |
| Cylinder    |  |  |  |  |  |  |
| Rectangular |  |  |  |  |  |  |
| Sinusoidal  |  |  |  |  |  |  |



(a)

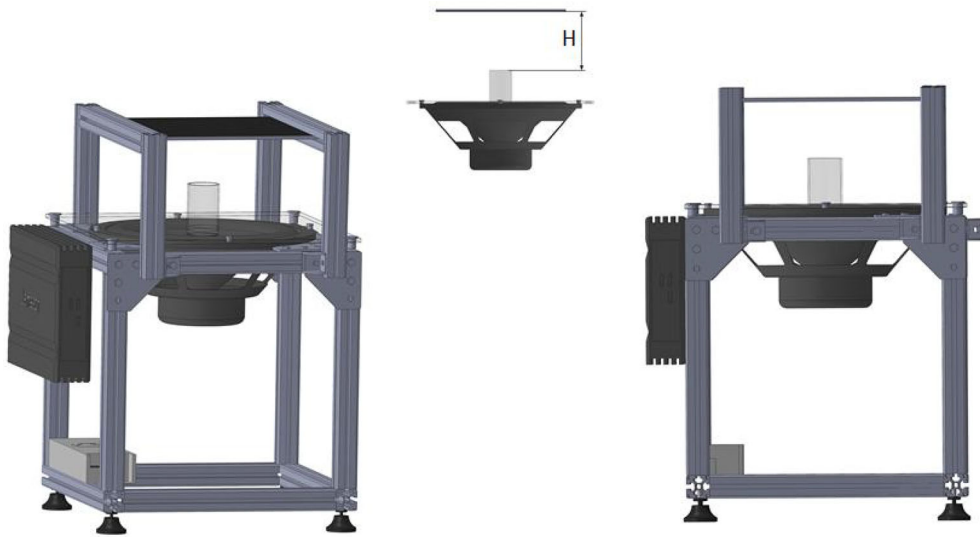


(b)

**Fig. 2** a 2D b 3D views of the Schlieren imaging experimental setup of the synthetic jet mechanism

this reason, the density difference is obtained by heating the speaker cavity and the images are recorded in this manner. The images are initially captured as a 1-min long video by using 12-megapixel camera with a 1080-pixel ( $1920 \times 1080$ ) image resolution and 30 fps frame rate. These videos are then used to capture the still images for visualization of the flow field. The still images captured from the videos are used to illustrate the initial, developed and fully developed vortex rings.

The jet structures at the orifice exit of the synthetic jet actuator mechanism are examined in 2D by Schlieren imaging method. The oil visualization technique is also performed to observe the 3D effect of the jet structure. The experimental setup of the visualization system with oil at the orifice exit of the synthetic jet mechanism is given in Fig. 3 with the CAD drawing. In this system, it is observed how the flow is distributed by applying an oil layer to the surface of the plate at the fixed position. A new system is designed for oil visualization of the synthetic jet actuator mechanism. In this system, a layer of oil is applied to the surface of a black plate positioned at a constant height  $H$ , to observe how the flow is distributed. The oil layer contains a mixture of titanium dioxide, oleic acid and kerosene with a ratio of 1:5:7. The used mixture



**Fig. 3** Top and side view of synthetic jet system for oil visualization

ratio used complies with the ones reported in the study of Sudhakar et al. (2019) and Seyhan and Sarioğlu (2021). In the process, titanium dioxide is added to the kerosene as a colourant, and a low-viscosity mixture is formed by adding oleic acid to ensure its homogeneity. Using this liquid white mixture, the distribution of the air on the black plate of the orifice jet is observed. With this oil visualization, the flow field distributions of different jet structures formed at different orifice geometric ratios are examined. The oil visualization method is very advantageous as it is an easy to apply and effective method. However, at very low velocity flows, the effect of the fluid flow may not be fully seen due to the viscosity of the mixture.

### 3 Result

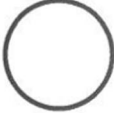

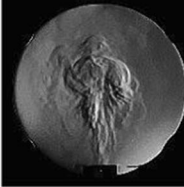
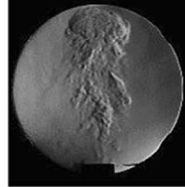
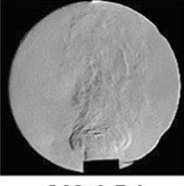
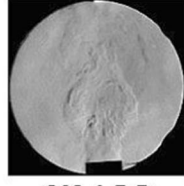
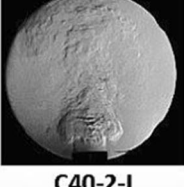
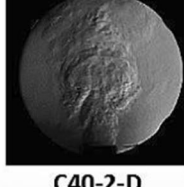
The Schlieren flow visualization method illustrates the formation of vortex rings in a synthetic jet structure. Images obtained in the Schlieren flow visualization method are presented in Tables 1, 2, 3, 4 and 5. Geometric parameters, excitation voltage, excitation frequency, excitation waveform geometric aspect ratios-related details are provided in the following sections.

#### 3.1 Effects of synthetic jet geometry



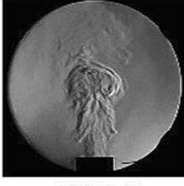


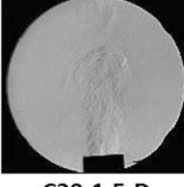
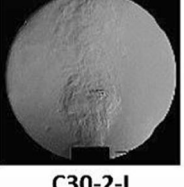
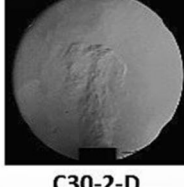
By using the synthetic jet actuator mechanism setup, the proposed geometric models and the related geometric ratios of the orifice structure are investigated. In this study, three different forms of geometrical structures, namely as cylindrical, rectangular and sinusoidal types, are evaluated. The Schlieren imaging method is used to observe the flow structures clearly. In Schlieren imaging, videos are taken at 1-min intervals after the synthetic jet actuator speaker cavity is heated. Pictures are obtained by photographing the captured videos. In the Schlieren imaging flow visualization method, jet structures are more prominently observed mainly due to the low excitation frequency and less heat dissipation at the applied voltage. The reason for this is that it is very difficult to observe the change in density difference as the frequency and voltage increases.

Gil and Strzelczyk (2016) measured the velocity of the orifice diameter change in the cylindrical geometry. As the diameter of the orifice geometry increased, the maximum velocity and the loudspeaker resonance frequency decreased. In this study, 24 mm orifice diameter loudspeaker resonance frequency  $U_0 = 4.8$  m/s is obtained. In addition, Gil (2017) examined the morphology of synthetic jet developmental stages of the 24 mm orifice diameter in his other study. In this study, the flow field is supported with analogy to the other work reported in literature. In the current study, different orifice geometries are used and it is observed that the geometric structure of the 20 mm cylinder orifice and the flow structure of Gil (2017) are similar. The study by Gil and Strzelczyk (2016) also included the speed measurements. As a result of this

**Table 3** Cylindrical synthetic jets,  $D = 40$  mm,  $V = 1, 1.5$  and  $2$  volts,  $f = 4$  Hz, wave type: square




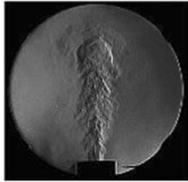

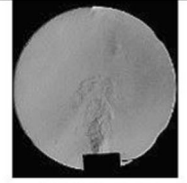
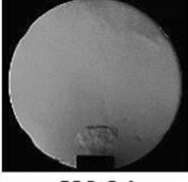
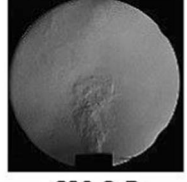
| Model   | Voltage   | Initial   | Developed  | Fully Developed  |
|---|-----------|---|--|--|
|  | 1 V       |  |   |  |
|   |           | C40-1-I   | C40-1-D  | C40-1-FD   |
|   |           | 1.5 V   |   |   |
|   | C40-1.5-I |   | C40-1.5-D  | C40-1.5-FD   |
|   | 2 V       |   |  |  |
|   |           | C40-2-I   | C40-2-D  | C40-2-FD   |

**Table 4** Cylindrical synthetic jets,  $D = 30$  mm,  $V = 1, 1.5$  and  $2$  Volts,  $f = 4$  Hz, wave type: square

| Model   | Voltage   | Initial   | Developed   | Fully Developed  |
|---|-----------|---|---|--|
|  | 1 V       |  |  |  |
|   |           | C30-1-I   | C30-1-D   | C30-1-FD   |
|   |           | 1.5 V   |  |   |
|   | C30-1.5-I |   | C30-1.5-D   | C30-1.5-FD   |
|   | 2 V       |   |  |   |
|   |           | C30-2-I   | C30-2-D   | C30-2-FD   |



**Table 5** Cylindrical synthetic jets,  $D = 20$  mm,  $V = 1, 1.5$  and  $2$  volts,  $f = 4$  Hz, wave type: square

| Model   | Voltage   | Initial   | Developed   | Fully Developed  |
|---|-----------|---|---|--|
|  | 1 V       |  |  |  |
|   |           | C20-1-I   | C20-1-D   | C20-1-FD   |
|   |           | 1.5 V   |  |   |
|   | C20-1.5-I |   | C20-1.5-D   | C20-1.5-FD   |
|   | 2 V       |   |  |   |
|   |           | C20-2-I   | C20-2-D   | C20-2-FD   |

study, it can be said that as the orifice diameter increases, the speed decreases, and as the orifice diameter decreases, the speed increases. Gil and Strzelczyk (2016) and Gil (2017) used a single orifice model in their studies, and there was an obvious need for analysis of other geometries. Therefore, in the current study, different aspect ratios of different geometric models are examined in order to better observe the change in flow fields. In literature, the study by Gil and Strzelczyk (2016) has a similar geometry and the reported results (for pressure or for velocity measurements) match with the presented study. The dimensionless parameters are used to check the results for compatibility. Not only are the geometric properties such as aspect ratios, but also electrical properties of the actuator are taken into account. Hence, the main focus of the study is set on the actual flow structure of the synthetic jets generated by using two different visualization techniques that sets the presented study apart from the similar studies reported.




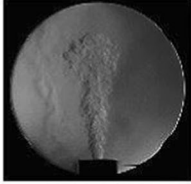
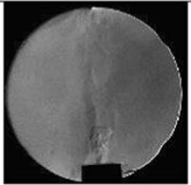
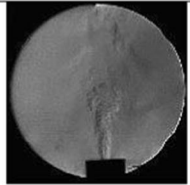
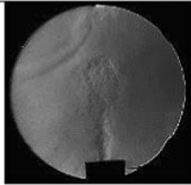
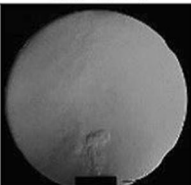
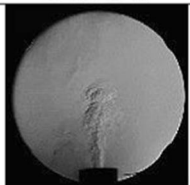
Tables 3, 4, 5, 6 and 7 show results of the examination of the applied voltage changes at an excitation frequency of 4 Hz for the cylindrical geometric structure achieved by Schlieren imaging flow visualization technique. Gil (2017) divided the formation phases of the vortex rings on the synthetic jet morphology at the orifice jet exit into five regime structures. In Gil's study, it is observed that in the 4th regime, a vortex ring formed in the synthetic jet and moved away from the hole with its self-induced speed. In the 5th regime, a strong turbulent synthetic jet was formed. It is stated that these two regimes are the most ideal synthetic jet structure due to the long-range effect. Also, the development of the flow structure at the initial stage, developed and fully developed regime is determined by the formation and propagation of a separate vortex ring under periodic reverse flow condition (Glezer and Amitay 2002).

The naming convention used in the tables created in the Schlieren imaging flow visualization is given in Fig. 4. In Tables 3, 4, 5, 6 and 7, the formation of vortex rings in geometric structures with different proportions of the cylindrical orifice model is examined in three main sections as initiation, developed and fully developed forms.


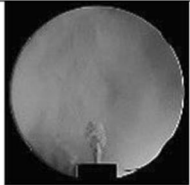


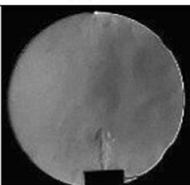
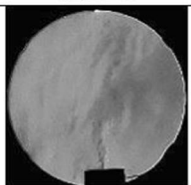
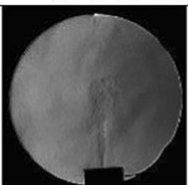
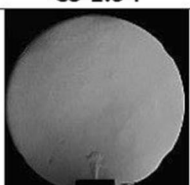
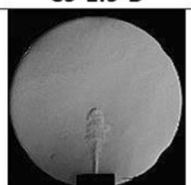
The observations are as follows;

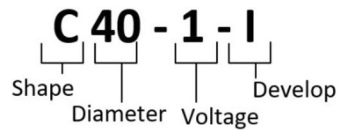
- The clearest vortex rings occur at the lowest applied voltage for the cylindrical orifice geometry.
- At 1 V application voltage, ruptures in vortex rings are observed in the C40-1-I, C40-1-D, C40-1-FD, C30-1-I, C30-1-D and C30-1-FD jet structures.

**Table 6** Cylindrical synthetic jets,  $D = 10$  mm,  $V = 1, 1.5$  and  $2$  volts,  $f = 4$  Hz, wave type: square

| Model   | Voltage | Initial  | Developed  | Fully Developed  |  |
|---|---------|--|--|--|--|
|  | 1 V     | <br>C10-1-I | <br>C10-1-D   | <br>C10-1-FD |  |
|   |         | 1.5 V  | <br>C10-1.5-I | <br>C10-1.5-D | <br>C10-1.5-FD |
|   |         |  | 2 V  | <br>C10-2-I   | <br>C10-2-D     |

**Table 7** Cylindrical synthetic jets,  $D = 5$  mm,  $V = 1, 1.5$  and  $2$  volts,  $f = 4$  Hz, wave type: square

| Model   | Voltage | Initial   | Developed   | Fully Developed   |   |
|---|---------|---|---|---|---|
|  | 1 V     | <br>C5-1-I | <br>C5-1-D   | <br>C5-1-FD |   |
|   |         | 1.5 V   | <br>C5-1.5-I | <br>C5-1.5-D | <br>C5-1.5-FD |
|   |         |   | 2 V   | <br>C5-2-I   | <br>C5-2-D     |



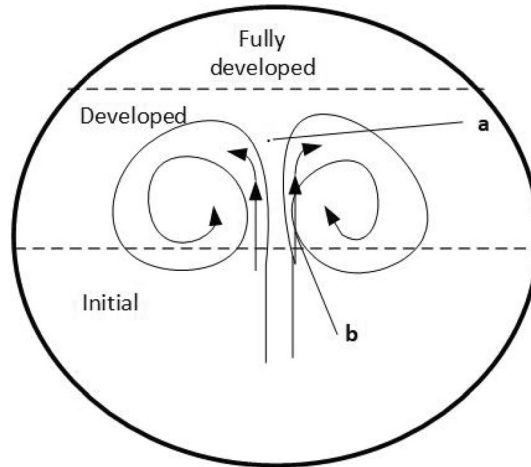
**Fig. 4** Details of the naming format of the pictures in the table

- At 1 V applied voltage, it is observed that the primary vortex ring effect persists in the initial phase at C40-1-I, C30-1-I and C20-1-I. However, the primary vortex ring effect is not observed in C10-1-I and C5-1-I.
- At 1 V, 1.5 V and 2 V application voltages, vortex rings are formed without jet rupture in all regimes from C10-1-I to C45 except C5-1-I.
- At 1 V, 1.5 V and 2 V application voltages, it is observed that vortex rings are divided into small vortices from C10-1-I to C45 except C5-1-I and vortex structures are formed.
- The vortex rings are considerably weakened in jet structure due to the very small geometry of the orifice models for C5-1-I to C45 at 1 V, 1.5 V and 2 V applied voltage. As the diameter decreases, a rapid jet exit occurs due to the increase in the speed passing through the orifice. That is, rapid vortex rings are formed. This causes the vortex rings extends upwards. For this reason, it caused the formation of small vortex structures.
- It is observed that the distribution of the vortex rings of the cylinder orifice geometric structure widens as the application voltage increases. In addition, as the voltage increases, it is observed that there is a weakening in the flow image due to its strong dominant effect.
- For 4 Hz 1 V in cylindrical structures, ideal vortex ring formation is observed for jet structure of 20 mm orifice geometry. The results obtained by the cylinder orifice geometric method in the study of Hong et al. (2020) support and confirm the flow structure formation observed for the 20 mm orifice geometry.
- The vortex rings formed in the C40-1-D picture support the jet structure in the synthetic jet from Gil (2017)'s morphology structures. In Fig. 5, the parts formed in the vortex ring structure are shown. As seen in Fig. 5, vortex rings formed in C40-1-D, and vortex structures were formed at the core point. In the C40-1-D picture, vortex rings are realized in the develop part. In the fully developed part of the C40-1-FD picture, it is seen that there are breaks at the exit of the synthetic jet. In addition, the effect of the second vortex ring is observed quite clearly.
- The vortex rings formed in the C8 picture are also similar to the Gil (2017) synthetic jet structure. However, since a faster jet is formed in this geometry, the vortex rings are formed in a more collected state. In this structure, vortex rings occurred at the core point in the developed part. As described in Hong (2020), it is observed that geometric parameter variability affects the change in vortex structures. Looking at the fully developed part of this structure, it is similar to the strong turbulent synthetic jet formation in Gil (2017).
- The vortex ring formation in the synthetic jet formed at C30-1-D and C40-1-D is similar in the develop section. Likewise, C30-1-FD and C40-1-FD are similar in fully develop section. However, due to the small diameters of C30-1-D and C30-1-FD, the vortex ring formation is more massive and it is observed that the ruptures were less at the jet exit.
- The jet structure formed in C20-1-FD is formed without breaking the jet structure in the fully developed image. It is observed that a new synthetic jet structure is formed with vortex rings in a highly combined structure. In this cylindrical geometric structure, the jet exit in the initial and develop part formed a smooth jet without breaking at the core point.
- Since there is a small jet exit in the C45, very small vortexes are formed in the vortex ring and a direct jet structure is realized.

Tables 8, 9, 10, 11 and 12 present the analysis of flow structures of synthetic jet structures of rectangular orifice geometry at 4 Hz constant frequency and different application voltages by Schlieren imaging method. Also, in Tables 8, 9, 10, 11 and 12, the initial, developed and fully developed stages of rectangular flow structures with different aspect ratios (AR = 8, 6, 4, 2, 1) are observed.


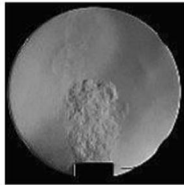
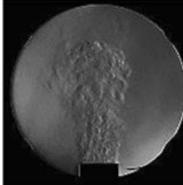
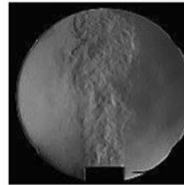
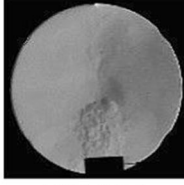
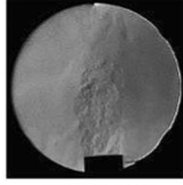
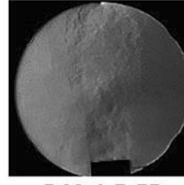
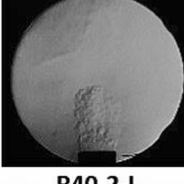
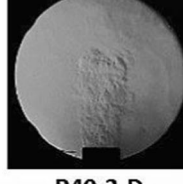
The observations are as follows;

- It is observed that a fairly flat jet structure is formed for the rectangular orifice geometry.




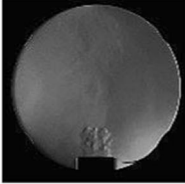
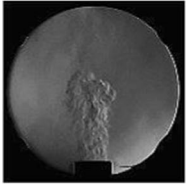
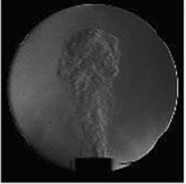
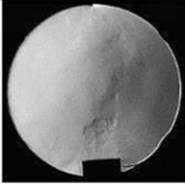
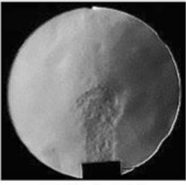
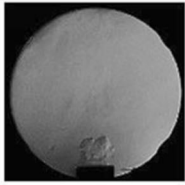
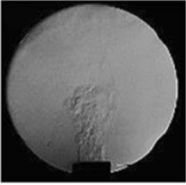
**Fig. 5** Vortex rings **a** Core point region **b** Direct jet structure

**Table 8** Rectangular synthetic jets,  $D = 40$  mm,  $V = 1, 1.5$  and  $2$  volts,  $f = 4$  Hz, wave type: square


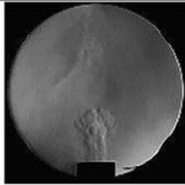
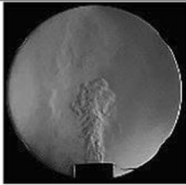

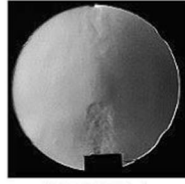
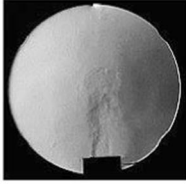
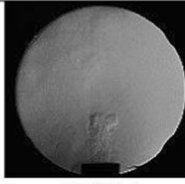
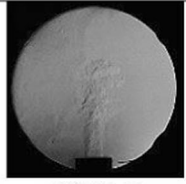
| Model   | Voltage | Initial   | Developed  | Fully Developed  |  |
|---|---------|---|--|--|--|
|  | 1 V     | <br>R40-1-I | <br>R40-1-D    | <br>R40-1-FD  |  |
|   |         | 1.5 V   | <br>R40-1.5-I | <br>R40-1.5-D | <br>R40-1.5-FD |
|   |         |   | 2 V  | <br>R40-2-I   | <br>R40-2-D     |

- It has been observed that there are no ruptures in the formation of jets in the far field regions of the structures from R40-1-I to R40-2-FD (except R40-1-FD) at 1 V, 1.5 V and 2 V application voltages. It is observed that a flat jet structure and small vortex structures are formed in this structure. The presence of sharp corners in the rectangular orifice geometric model leads to a self-induced velocity. It reaches a higher speed in areas close to sharp corners and moves faster than in other sections. This speed difference lengthens the vortex ring and causes it to move away from the centre.
- As the aspect ratio of the rectangular orifice geometry decreases, it resembles the vortex rings formed in the cylindrical orifice geometry. Particular similarity is observed in structures from R5-1-I to R5-2-FD as the rectangular orifice geometric model ( $AR = 1$ ) has deformed into a square geometric model due to the aspect ratio. The square hole geometry with  $AR = 1$  is very similar to the circular hole geometry.

**Table 9** Rectangular synthetic jets,  $D = 30$  mm,  $V = 1, 1.5$  and  $2$  volts,  $f = 4$  Hz, wave type: square


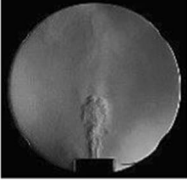

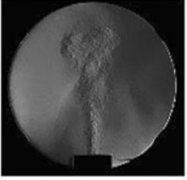
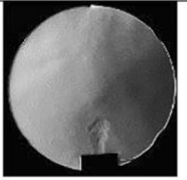
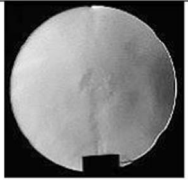



| Model   | Voltage   | Initial   | Developed   | Fully Developed  |
|---|-----------|---|---|--|
|  | 1 V       |  |  |  |
|   |           | R30-1-I   | R30-1-D   | R30-1-FD   |
|   |           | 1.5 V   |  |   |
|   | R30-1.5-I |   | R30-1.5-D   | R30-1.5-FD   |
|   | 2 V       |   |  |   |
|   |           | R30-2-I   | R30-2-D   | R30-2-FD   |

**Table 10** Rectangular synthetic jets,  $D = 20$  mm,  $V = 1, 1.5$  and  $2$  volts,  $f = 4$  Hz, wave type: square



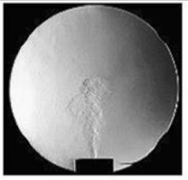
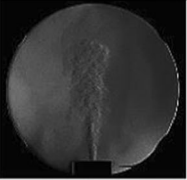
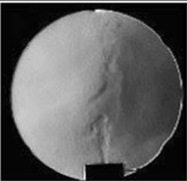

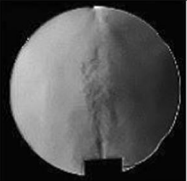
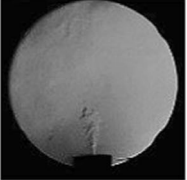

| Model   | Voltage   | Initial   | Developed   | Fully Developed  |
|---|-----------|---|---|--|
|  | 1 V       |  |  |  |
|   |           | R20-1-I   | R20-1-D   | R20-1-FD   |
|   |           | 1.5 V   |  |   |
|   | R20-1.5-I |   | R20-1.5-D   | R20-1.5-FD   |
|   | 2 V       |   |  |   |
|   |           | R20-2-I   | R20-2-D   | R20-2-FD   |

Especially since R5-2-FD has the smallest geometric ratio in the rectangular structure and a fast jet output, direct jet output has been realized. In the study of Wang et al. (2017), it was stated that the

**Table 11** Rectangular synthetic jets,  $D = 10$  mm,  $V = 1, 1.5$  and  $2$  volts,  $f = 4$  Hz, wave type: square

| Model   | Voltage | Initial  | Developed  | Fully Developed  |  |
|---|---------|--|--|--|--|
|  | 1 V     | <br>R10-1-I | <br>R10-1-D   | <br>R10-1-FD |  |
|   |         | 1.5 V  | <br>R10-1.5-I | <br>R10-1.5-D | <br>R10-1.5-FD |
|   |         |  | 2 V  | <br>R10-2-I   | <br>R10-2-D     |

**Table 12** Rectangular synthetic jets,  $D = 5$  mm,  $V = 1, 1.5$  and  $2$  volts,  $f = 4$  Hz, wave type: square

| Model   | Voltage | Initial   | Developed   | Fully Developed   |   |
|---|---------|---|---|---|---|
|  | 1 V     | <br>R5-1-I | <br>R5-1-D   | <br>R5-1-FD |   |
|   |         | 1.5 V   | <br>R5-1.5-I | <br>R5-1.5-D | <br>R5-1.5-FD |
|   |         |   | 2 V   | <br>R5-2-I   | <br>R5-2-D     |


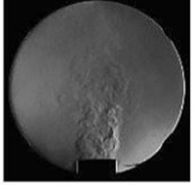
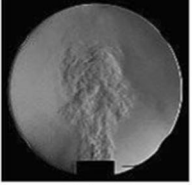
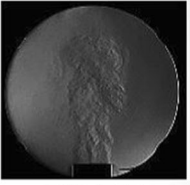
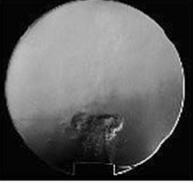
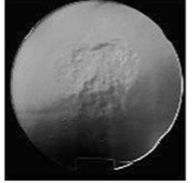
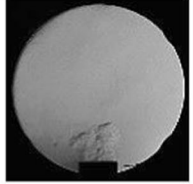
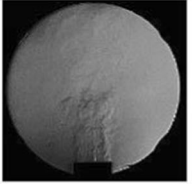
cylindrical orifice geometric structure is quite similar to each other in the square orifice geometry with low AR structure.

- When the fully developed structures are examined, it is observed that the vortex rings turned into small vortex structures in the far field region in R20-1-FD, R24, R27, R10-1-FD, R10-1.5-FD, R10-2-FD, R5-1-FD, R5-1.5-FD and R5-2-FD.
- In the R40-1-D develop image, the vortex ring image is more compact than the cylindrical structure, or a flat jet exit is formed.
- In the R30-1-FD fully develop image, the vortex ring formation is more pronounced above the core point than in R40-1-FD.
- When the R40-1-FD, R30-1-FD and R20-1-FD fully develop images are compared, the vortex ring becomes more prominent and more similar to the cylindrical geometric structure as the geometric ratio of the rectangle decreases. Especially in the R20-1-FD fully develop picture, the vortex ring was realized quite clearly at the core point indicated in Fig. 4.
- In the rectangular models of the R20-1-FD and R10-1-FD images, the best images are obtained in the formation of the vortex ring.


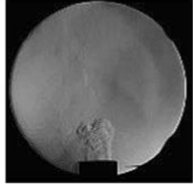
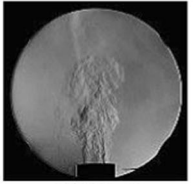
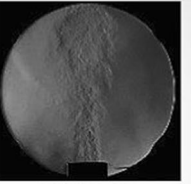
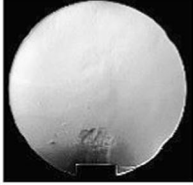
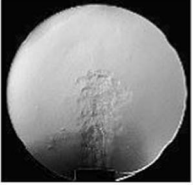
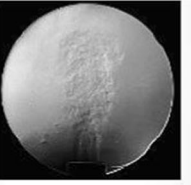
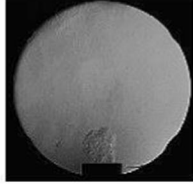
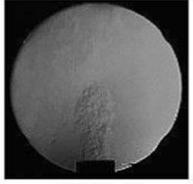
Tables 13, 14, 15, 16 and 17 provide the details of the examination of the flow structures of the synthetic jet in a sinusoidal orifice geometric model at a constant frequency of 4 Hz and different application voltages by Schlieren imaging method. Also, in Tables 13, 14, 15, 16 and 17, flow visualization images of initial, developed and fully developed vortex formation regime of sinusoidal orifice geometric models in different aspect ratios (AR = 8, 6, 4, 2, 1) are given.

- Sinusoidal jet geometry is a new jet structure. In the sinusoidal orifice geometry, it is observed that the jet structures are formed as “S” waves in the images from S40-1-I to S30-2-FD. In Fig. 6, the formation of the “S” form is seen in detail in the S30-1-D picture.
- In the sinusoidal orifice geometric structure, the forms of AR = 1 and AR = 2 structures are similar to the circular structure forms. For this reason, it is seen that the structures from S20-1-I to S5-2-FD are quite similar to the structures from C10-1-I to C5-2-FD in cylindrical orifice geometry.
- The effect of the “S” type jet structure continues from S40-1-I 1 to S5-2-FD.


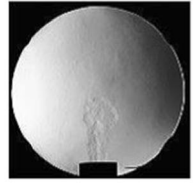
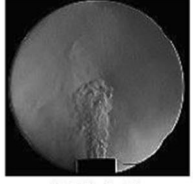
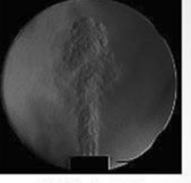
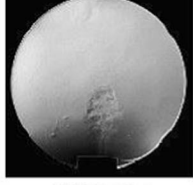
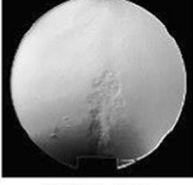
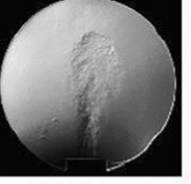
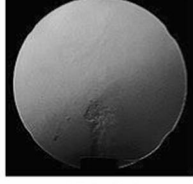
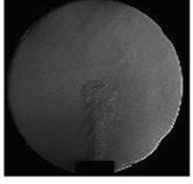
**Table 13** Sinusoidal synthetic jets, D = 40 mm, V = 1, 1.5 and 2 volts, f = 4 Hz, wave type: square

| Model   | Voltage          | Initial   | Developed   | Fully Developed  |
|---|------------------|---|---|--|
|  | <b>1 V</b>       |  |  |  |
|   |                  | <b>S40-1-I</b>  | <b>S40-1-D</b>  | <b>S40-1-FD</b>  |
|   |                  | <b>1.5 V</b>  |  |   |
|   | <b>S40-1.5-I</b> |   | <b>S40-1.5-D</b>  | <b>S40-1.5-FD</b>  |
|   | <b>2 V</b>       |   |  |   |
|   |                  | <b>S40-2-I</b>  | <b>S40-2-D</b>  | <b>S40-2-FD</b>  |

**Table 14** Sinusoidal synthetic jets,  $D = 30$  mm,  $V = 1, 1.5$  and  $2$  volts,  $f = 4$  Hz, wave type: square


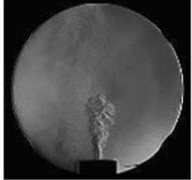
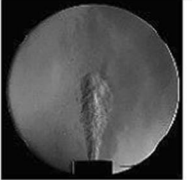
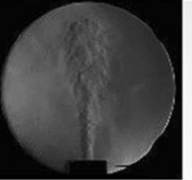
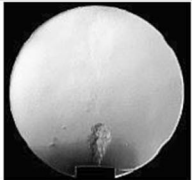
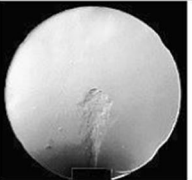
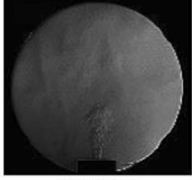
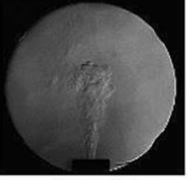
| Model   | Voltage | Initial  | Developed  | Fully Developed  |  |
|---|---------|--|--|--|--|
|  | 1 V     | <br>S30-1-I | <br>S30-1-D   | <br>S30-1-FD |  |
|   |         | 1.5 V  | <br>S30-1.5-I | <br>S30-1.5-D | <br>S30-1.5-FD |
|   |         |  | 2 V  | <br>S30-2-I   | <br>S30-2-D     |

**Table 15** Sinusoidal synthetic jets,  $D = 20$  mm,  $V = 1, 1.5$  and  $2$  volts,  $f = 4$  Hz, wave type: square


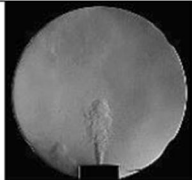

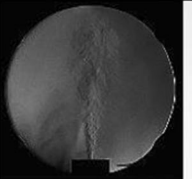
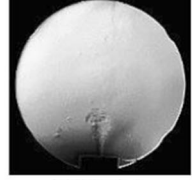
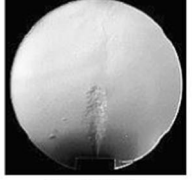
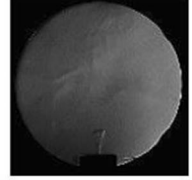
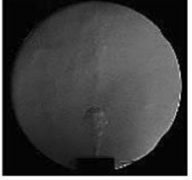
| Model   | Voltage | Initial  | Developed  | Fully Developed  |  |
|---|---------|--|--|--|--|
|  | 1 V     | <br>S20-1-I | <br>S20-1-D   | <br>S20-1-FD |  |
|   |         | 1.5 V  | <br>S20-1.5-I | <br>S20-1.5-D | <br>S20-1.5-FD |
|   |         |  | 2 V  | <br>S20-2-I   | <br>S20-2-D     |



**Table 16** Sinusoidal synthetic jets,  $D = 10$  mm,  $V = 1, 1.5$  and  $2$  volts,  $f = 4$  Hz, wave type: square

| Model   | Voltage   | Initial   | Developed   | Fully Developed  |
|---|-----------|---|---|--|
|  | 1 V       |  |  |  |
|   |           | S10-1-I   | S10-1-D   | S10-1-FD   |
|   |           | 1.5 V   |  |   |
|   | S10-1.5-I |   | S10-1.5-D   | S10-1.5-FD   |
|   | 2 V       |   |  |   |
|   |           | S10-2-I   | S10-2-D   | S10-2-FD   |

**Table 17** Sinusoidal synthetic jets,  $D = 5$  mm,  $V = 1, 1.5$  and  $2$  volts,  $f = 4$  Hz, wave type: square

| Model   | Voltage  | Initial   | Developed   | Fully Developed  |
|---|----------|---|---|--|
|  | 1 V      |  |  |  |
|   |          | S5-1-I  | S5-1-D  | S5-1-FD  |
|   |          | 1.5 V   |  |   |
|   | S5-1.5-I |   | S5-1.5-D  | S5-1.5-FD  |
|   | 2 V      |   |  |   |
|   |          | S5-2-I  | S5-2-D  | S5-2-FD  |

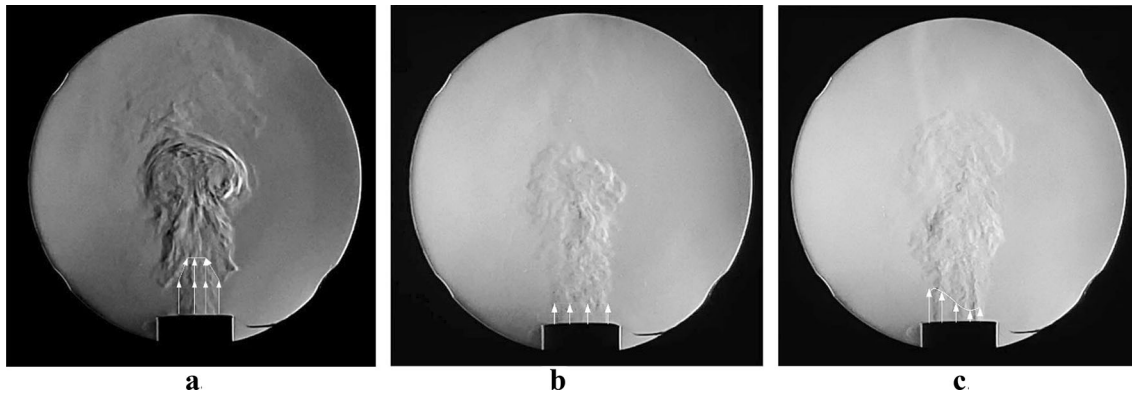


**Fig. 6** “S” wave formed in S30-1-D in sinusoidal orifice geometry

- In the S40-1-FD, S40-1.5-D and S40-2-FD structures, ruptures occur in the vortex structure in the far field region.
- The rupture intensity of the Eddy structures in the far field region of S30-1-I, S30-1.5-FD and S30-2-FD decreases compared to the S40-1-FD, S40-1.5-FD and S40-2-FD structures.
- In the jet structures from S20-1-I to S5-2-FD (except S20-1-FD and S10-1-FD 30), the formation of vortex rings occurred quite smoothly and without rupture.
- It is observed that a clear vortex structure is formed between S5-1-I and S5-2-FD. However, due to the small aspect ratio in the fully developed regime, the vortex structure seems to be weakened.
- As the aspect ratio decreases in the cylindrical geometric structure and vortex ring formation begins. With the decrease in the aspect ratio, the wave disturbances of the geometric structure disappear and the vortex ring formation takes place.
- A gradual vortex ring disappears as seen in S20-1-FD in the S10-1-FD fully developed picture.
- The S10-1.5-FD structure is very similar to the C20-1-FD structure. This, after a certain aspect ratio, increases its similarity to the cylindrical geometric structure.

Figure 7 shows equal velocity distribution from each region at the first exit. Then, by elongation from the sides, a narrowing occurs and a vortex ring is formed. As can be seen in Tables 3, 4, 5, 6 and 7, the ratio of vortex rings in decreasing aspect ratio also turns into a very small vortex. In Fig. 7b, in the synthetic jet mechanism, it has been observed that the short side moves faster than the long side while a vortex ring emerges from a rectangular orifice. Here, it creates a vortex by going towards the centre of the vortex ring on the short side and elongates it upwards from the centre on the long side. As can be seen in Tables 8, 9, 10, 11 and 12, when the aspect ratio decreases, the speed difference between the short and long sides decreases and the vortex ring formation is observed to become increasingly different. In Fig. 7, in the sinusoidal jet geometry, an exit occurs while preserving the “s” form at the first jet exit. However, due to the velocity difference between the long sides of the s-form in the circle part and the short side as the jet rises, the vortex formation starts from its short sides, and the vortex ring spreads upwards. This causes the formation of a vortex ring in an expanding structure of the upward s-form. As can be seen in Tables 13, 14, 15, 16 and 17, there are differences in the structures of the vortex rings according to the decreasing aspect ratio of the sinusoidal geometric structure.

In square signal wave form, the related actuator membrane motion leads to higher mass flow ratio compared to other signal types. As a result, the synthetic jet generated has a stronger effect. This is observed in the Schlieren imaging results as clear jets with larger height properties. In geometric models, as the aspect ratio decreases, the amount of air it will take in decreases and the displacement of the actuator is reduced in magnitude. The direct jet structures are formed due to the formation of less momentum. However, when looking at geometries with high aspect ratio, vortex rings are formed quite clearly due to the high momentum effects.



**Fig. 7** a C11 cylinder geometric jet b R11 rectangular geometric jet c S11 sinusoidal geometric jet

### 3.2 Effect of excitation voltage

In the study, the effect of the applied voltage on the synthetic jet flow structure is also investigated. The applied voltage is defined as 1, 1.5 and 2 Volts. The vortex structures are better observed when Schlieren imaging is performed with the lower end of the applied frequency and lower end of the voltage ranges in the flow visualization. Therefore, the oil visualization is performed for these range of settings.

The distribution of the excitation application voltage of the synthetic jet actuator in different aspect ratios of cylindrical, rectangular and sinusoidal geometric structures is shown in Tables 18, 19 and 20. As shown in the Schlieren imagine visualization of the cylindrical orifice geometry in Table 18, it is observed that the smaller the diameter, the smaller the flow domain, but a stronger the flow. In the oil visualization experiment, as the aspect ratio decreased, it creates a stronger effect area due to the formation of a direct jet structure. Looking at high aspect ratio geometries, Schlieren imaging provides clear vortex rings in flow visualization, while in oil visualization the flow area widens, the impact force decreases. In addition, it is observed that in structures with aspect ratio  $AR = 4$  and  $2$ , it forms a smooth vortex ring in Schlieren imaging and has a very wide and effective area of effect in oil visualization.

The details presented in Table 19 show the experimental results of oil visualization of geometric models of rectangular orifice shape in different aspect ratios. Due to the sharp corners in the rectangular orifice geometric structure, the vortex area is wider than the cylindrical orifice geometric structure. Oren et al. (2009) support that the propagation speed produced from the rectangular hole is higher than the square and circular orifice structure. In addition, it has been observed that the vortex areas formed in  $AR = 1$  square hole, and the hole geometries are similar. Among the rectangular orifice geometric structures, it is seen that the velocity is higher and the impact area is wider at  $AR = 4$ . It is seen that the effect of the vertical area is

**Table 18** Schlieren imaging and oil visualization of cylindrical geometric structures at 4 Hz 1 V

|                                | 40 mm | 30 mm | 20 mm | 10 mm | 5 mm |
|--------------------------------|-------|-------|-------|-------|------|
| Cylinder Orifice               |       |       |       |       |      |
| Schlieren Imaging Full Develop |       |       |       |       |      |
| Oil visualization Square Wave  |       |       |       |       |      |

**Table 19** Schlieren imaging and oil visualization of rectangular geometric structures at 4 Hz

|                                       | 40 mm | 30 mm | 20 mm | 10 mm | 5 mm |
|---------------------------------------|-------|-------|-------|-------|------|
| <b>Rectangular Orifice</b>            |       |       |       |       |      |
| <b>Schlieren Imaging Full Develop</b> |       |       |       |       |      |
| <b>Oil visualization Square Wave</b>  |       |       |       |       |      |



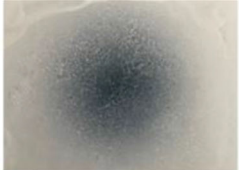
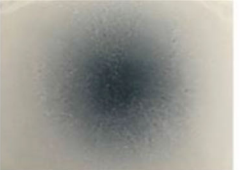


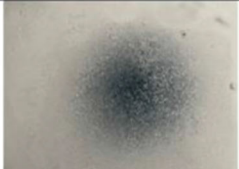
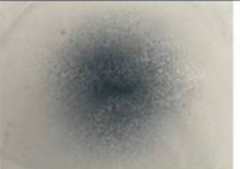

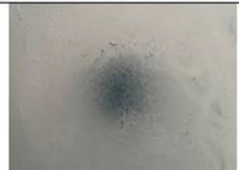
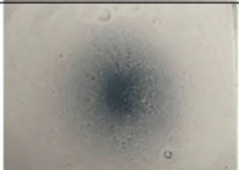
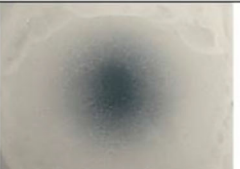
**Table 20** Schlieren imaging and oil visualization of sinusoidal geometric structures at 4 Hz 1 V

|                                       | 40 mm | 30 mm | 20 mm | 10 mm | 5 mm |
|---------------------------------------|-------|-------|-------|-------|------|
| <b>Sinusoidal Model</b>               |       |       |       |       |      |
| <b>Schlieren Imaging Full Develop</b> |       |       |       |       |      |
| <b>Oil visualization Square Wave</b>  |       |       |       |       |      |

quite low in rectangular orifice geometric  $AR = 1$ . It was observed that rectangular orifice geometry with aspect ratio  $AR = 8$  creates a greater impact area than  $AR = 8$  cylindrical orifice geometric structure. In rectangular orifice geometric models, as the aspect ratio decreases, the impact force is higher due to the formation of a direct jet structure and the area it affects decreases.

In Table 20, the results for Schlieren imaging and oil visualization of sinusoidal geometric structures at 4 Hz frequency and 1 V applied voltage are presented. To examine the Eddy field distribution in the synthetic jet actuator, the sinusoidal hole geometric structures are tested by using the oil visualization method. When the oil visualizations of the sinusoidal perforated geometric structure are examined, the propagation of the “S” wave in  $AR = 8$  and 6 is more pronounced than in  $AR = 4, 2$  and 1. As the aspect ratio decreases, the vortex rings decrease and the “S” structure form changes because the vortex rings form a more uniform jet structure. In addition, it has an effect on the change of the cylindrical orifice geometric structure form by reducing the aspect ratio. The similarity of the sinusoidal orifice geometric model to the cylindrical orifice geometric model increases as the aspect ratio decreases. As with cylindrical geometry, the area of effect of the oil visualization decreases as the aspect ratio decreases. However, in  $AR = 1$ , unlike the cylindrical orifice geometry, a second vortex effect is observed in the sinusoidal orifice geometric model. As seen in the Schlieren image and oil visualization, it is due to the formation of the second vortex ring while the effect of the primary vortex ring preserves itself. This is due to excessive circulation that cannot be suppressed by the primary vortex ring.



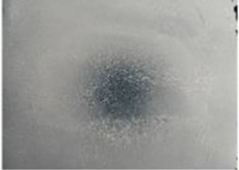
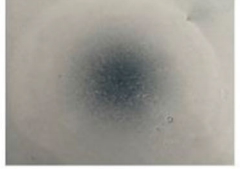

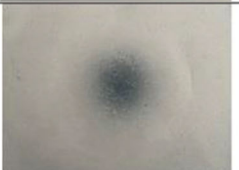
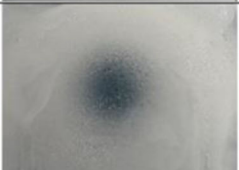


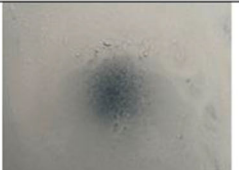
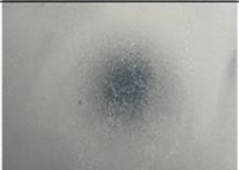

**Table 21** Flow structure changes with voltage change in geometric structure of 20 mm at constant frequency and square wave

| GEOMETRIC MODEL   | 1 V   | 1.5 V   | 2 V  |
|---|---|---|--|
|  |  |  |  |
|  |  |  |  |
|  |  |  |  |

Gil (2017) stated that ideal synthetic jet structure is formed when the vortex ring of the synthetic jet is self-induced in the 4th regime of the morphology structures of the jet, and a strong turbulent synthetic jet is formed in the 5th regime. In this study, when fully developed stages are examined, it is observed that the most suitable geometry is formed in geometric models with 20 mm orifice. The variation images of the application voltage in the 20 mm geometric model of cylindrical, rectangular and sinusoidal orifice geometries are given in Table 21.

- It has been observed that it makes quite a difference in the effect area between 1v and 1.5v. However, when looking between 1.5 and 2 V, there is a small change in the effect area. As a result, with the effect

**Table 22** Flow structure changes with frequency change in 20 mm geometric structure at fixed frequency and square wave

| GEOMETRIC MODEL   | 4 Hz  | 6 Hz  | 8 Hz   |
|---|---|---|--|
|  |  |  |  |
|  |  |  |  |
|  |  |  |  |

of voltage, the affected areas of all jet geometries expand by 1.5 V. After 1.5 V, it is observed that the change in the domains is very low or there will be no change in the domains.

- The cylindrical model has a very large distribution flow area in the form of a circle. In the rectangular model, a rectangular flow distribution area is formed. While the flow distribution area of the rectangular model is formed, it has been observed that the flow spreading from the long side gives a longer length than the flow spreading from the short side. The sinusoidal model has an oval flow distribution area.
- When 3 different orifice geometric models were compared, the vertical area distribution of the cylindrical orifice geometric model at 4 Hz 1.5 V spread over a wider area than other orifice models.

### 3.3 Effect of excitation frequency

In this study, the effect of the changes in the excitation frequency as 4 Hz, 6 Hz and 8 Hz in 3 different orifice geometric models are investigated. Considering the morphology presented by Gil (2017), since geometric models with 20 mm orifices have ideal vortex structures, the different excitation frequency changes in geometric models at constant voltage in Table 20 are examined by Schlieren imaging and oil visualization techniques.

In Table 22, the results of the study for the frequency variation of the fixed voltage at 4, 6 and 8 Hz at 20 mm geometric ratio of 3 different models are illustrated.

The observations are as follows:

- When the cylindrical, rectangular and sinusoidal orifice geometric models are examined at constant frequency and voltage, it is seen that the vertical area distribution of the cylindrical model is wider than the other models.
- It is also observed that there is no effective difference in the flow area as the frequency increases for 1 V, 1.5 V and 2 Volts in geometric models with cylindrical, rectangular and sinusoidal holes. The reason for this is that the increase in frequency reduces the formation time of the flow field rather than increasing the flow field.

## 4 Conclusion

In this study, the flow field properties of the flow produced in different orifice geometries using a loud-speaker type synthetic jet actuator are investigated. The geometric length of the orifice is defined as 40, 30, 20, 10 and 5 mm, and it is examined in cylindrical, rectangular and sinusoidal geometric model forms. The square signal type is used to generate the movement of the actuator diaphragm in synthetic jet generation. Frequency values of 4, 6 and 8 Hz and 1, 1.5 and 2 V of application voltage are studied. This Schlieren and oil visualization study is used for determination of flow field regimes.

- In Schlieren imaging visualization, the best images are observed at the lowest electrical parameter (4 Hz frequency and 1 volts voltage levels).
- At 1 V, 1.5 V and 2 V application voltages, vortex rings are formed without jet rupture in all regimes from C20-1-I to C45, R19 to R5-2-FD and S19 to S5-2-FD.
- It forms as “S” waves in the images from S40-1-I to S30-2-FD, and a flat jet output is seen in the images from R40-1-I to R40-2-FD.
- It is observed that the model, which develops in the smoothest structure in cylindrical, rectangular and sinusoidal geometric structures, occurs in geometric structures of  $C = R = S = 20$  mm.
- When the Schlieren and oil visualizations are examined in the circular, rectangular and sinusoidal orifice geometries at  $C = R = S = 5$  mm, it is observed that very similar structures are formed.
- Cylindrical, rectangular and sinusoidal orifice models form a circular, rectangular and oval vertical area distribution, respectively.
- In geometric models with cylindrical, rectangular and sinusoidal orifice, the flow area increases with increasing applied voltage.
- At constant frequency and applied voltage, the cylindrical orifice geometric model has a wider vertical area distribution than the other perforated models.

The presented study provides results to clarify the details of flow characteristics in cylindrical, rectangular and sinusoidal orifice geometries in synthetic jet formation. It is important to note that the effects of different vortex rings occur in different orifice geometries in the synthetic jet mechanism. The study of the effects of flow fields in various synthetic jet geometries contributes to the literature for future studies on impact synthetic jet applications. In future research, flow fields are expected to contribute to the investigation of the flow phenomenon in multi-actuator-based jet structure interactions, where essentially improved heat transfer and better cooling effects are needed.

## References

- Broučková Z, Trávníček Z (2014) Visualization study of hybrid synthetic jets. *J vis* 18(4):581–593. <https://doi.org/10.1007/s12650-014-0256-8>
- Broučková Z, Trávníček Z (2019) Intermittent round jet controlled by lateral pulse-modulated synthetic jets. *J vis* 22:459–476. <https://doi.org/10.1007/s12650-019-00550-z>
- Cater JE, Soria J (2002) The evolution of round zero-net-mass-flux jets. *J Fluid Mech* 472:167–200. <https://doi.org/10.1017/s0022112002002264>
- Chaudhari M, Bhalchandra P, Agrawal A (2010) Heat transfer characteristics of synthetic jet impingement cooling. *Int J Heat Mass Transf* 53(5–6):1057–1069. <https://doi.org/10.1016/j.ijheatmasstransfer.2009.11.005>
- Chaudhry IA, Zhong S (2014) A single circular synthetic jet issued into turbulent boundary layer. *J vis* 17(2):101–111. <https://doi.org/10.1007/s12650-014-0199-0>
- Dauphinee TM (1957) Acoustic air pump. *Rev Sci Instrum* 28(6):456. <https://doi.org/10.1063/1.1715904>
- Didden N (1979) On the formation of vortex rings: rolling-up and production of circulation. *Zeitschrift Für Angewandte Mathematik Und Physik ZAMP* 30:101–116. <https://doi.org/10.1007/bf01597484>
- Duan T, Wang J (2015) Experimental investigation on the evolution of axi-symmetrical synthetic jet. *J vis* 19(3):351–358. <https://doi.org/10.1007/s12650-015-0322-x>
- Fanning E, Persoons T, Murray DB (2015) Heat transfer and flow characteristics of a pair of adjacent impinging synthetic jet. *Int J Heat Fluid Eng* 54:153–166. <https://doi.org/10.1016/j.ijheatfluidflow.2015.08.001>
- Farnsworth JAN, JvC V, Amitay M (2008) Active flow control at low angles of attack: stingray unmanned aerial vehicle. *AIAA J* 46:10. <https://doi.org/10.2514/1.35860>
- Feero MA, Lavoie P, Sullivan PE (2015) Influence of cavity shape on synthetic jet performance. *Sens Actuator A Phys* 233:1–10. <https://doi.org/10.1016/j.sna.2014.12.004>
- Feero MA, Lavoie P, Sullivan PE (2016) Three-dimensional span effects of high-aspect ratio synthetic jet forcing for separation control on a low Reynolds number airfoil. *J vis* 20(1):45–51. <https://doi.org/10.1007/s12650-016-0365-7>
- Genç MS, Kaynak Ü, Yapici H (2011) Performance of transition model for predicting low aerofoil flows without/with single and simultaneous blowing and suction. *Eur J Mech B Fluids* 30:218–235. <https://doi.org/10.1016/j.euromechflu.2010.11.001>
- Gil P, Strzelczyk P (2016) Performance and efficiency of loudspeaker driven synthetic jet actuator. *Exp Therm Fluid Sci* 76:163–174. <https://doi.org/10.1016/j.expthermflusci.2016.03.020>
- Gillarranz JL, Traub LW, Rediniotis OK (2005) A new class of synthetic jet actuators-part II: application to flow separation control. *J Fluids Eng* 127(2):377–387. <https://doi.org/10.1115/1.1882393>
- Glezer A, Amitay M (2002) Synthetic jets. *Annu Rev Fluid Mech* 3:503–529. <https://doi.org/10.1146/annurev.fluid.34.090501.094913>
- Goodfellow SD, Yarusevych S, Sullivan PE (2013) Smoke-wire flow visualization of a synthetic jet. *J vis* 16:9–12. <https://doi.org/10.1007/s12650-012-0155-9>
- Holman R, Utturkar Y, Mittal R, Smith BL, Cattafesta L (2005) Formation criterion for synthetic jets. *AIAA J* 43(10):2110–2116. <https://doi.org/10.2514/1.12033>
- Hong MH, Cheng SY, Zhong S (2020) Effect of geometric parameters on synthetic jet: a review. *Phys Fluids* 32(3):031301. <https://doi.org/10.1063/1.5142408>
- Ingard U, Labate S (1950) Acoustic circulation effects and the nonlinear impedance of orifices. *J Acoust Soc Am* 22(2):211–218. <https://doi.org/10.1121/1.1906591>
- Jeng TM, Hsu WT (2016) Experimental study of mixed convection heat transfer on the heated plate with the circular-nozzle synthetic jet. *Int J Heat Mass Transf* 97:559–568. <https://doi.org/10.1016/j.ijheatmasstransfer.2016.02.029>
- Kim W, Kim S, Choi K, Kim C (2010) Experimental and computational study on flow characteristics by synthetic jets configuration. In: 48th AIAA aerospace sciences meeting including the new horizons forum and aerospace exposition <https://doi.org/10.2514/6.2010-864>
- Kumar A, Saha AK, Panigrahi PK, Karn A (2021) The mechanism of vortex bifurcation vis-à-vis axial switching in rectangular synthetic jets. *Eur J Mech B Fluids* 86:78–89. <https://doi.org/10.1016/j.euromechflu.2020.12.002>
- Lighthill MJ (1978) Acoustic streaming. *J Sound Vib* 61:391–418. [https://doi.org/10.1016/0022-460X\(78\)90388-7](https://doi.org/10.1016/0022-460X(78)90388-7)
- Lin CY, Bai CJ, Hsiao FB (2014) An investigation on fundamental characteristics of excited synthetic jet actuator under cavity and diaphragm resonances. *Procedia Eng* 79:35–44. <https://doi.org/10.1016/j.proeng.2014.06.306>
- Mallinson SG, Reizes JA, Hong G, Westbury PS (2004) Analysis of hot-wire anemometry data obtained in a synthetic jet flow. *Exp Therm Fluid Sci* 28:265–272
- Mohseni K (2004) Zero-mass pulsatile jets for unmanned underwater vehicle maneuvering. In: AIAA 3rd “unmanned unlimited” technical conference, workshop and exhibit <https://doi.org/10.2514/6.2004-6386>

- Murugan T, Deyashi M, Dey S, Rana SC, Chatterjee PK (2016) Recent developments on synthetic jets. *Def Sci J* 66(5):489. <https://doi.org/10.14429/dsj.66.9776>
- Oren L, Gutmark E, Muragappan S, Khosla S (2009) Flow characteristics of non-circular synthetic jets. In: 47th AIAA aerospace sciences meeting including the new horizons forum and aerospace exposition <https://doi.org/10.2514/6.2009-1309>
- Ozkan G (2016) Investigation of unstable aerodynamics over wing at low Reynolds number flows. Thesis, University of Erciyes, Kayseri, Turkey, M.Sc
- Paweł GIL (2017) Morphology of synthetic jet. *Rutmec T. XXXIV, Kwiecień-Czerwiec* 89(2/2017):43–51. <https://doi.org/10.7862/rm.2017.15>
- Persoons T, McGuinn A, Murray DB (2011) A general correlation for the stagnation point nusselt number of an axisymmetric impinging synthetic jet. *Int J Heat Mass Transf* 54(17–18):3900–3908. <https://doi.org/10.1016/j.ijheatmasstransfer.2011.04.037>
- Seyhan M, Sarioglu M (2021) Investigation of drag reduction performance of half NACA 0009 and 0012 airfoils placed over a trailer on the flow around truck-trailer. *J Mech Sci Technol* 35(7):2971–2979. <https://doi.org/10.1007/s12206-021-0620-2>
- Smith BL, Swift GW (2001) Synthetic jets at large Reynolds number and comparison to continuous jets. In: 15th AIAA computational fluid dynamics conference <https://doi.org/10.2514/6.2001-3030>
- Smith BL, Glezer A (1998) The formation and evolution of synthetic jets. *Phys Fluids* 10(9):2281–2297. <https://doi.org/10.1063/1.869828>
- Sudhakar S, Karthikeyan N, Suriyanarayanan P (2019) Experimental studies on the effect of leading-edge tubercles on laminar separation bubble. *AIAA J* 54:12. <https://doi.org/10.2514/1.j058294>
- Tesař V, Trávníček Z (2005) Pulsating and synthetic impinging jets. *J vis* 8(3):201–208. <https://doi.org/10.1007/bf03181497>
- Trávníček Z, Broučková Z, Kordík J, Kordík J, Vít T (2015) Visualization of synthetic jet formation in air. *J vis* 18:595–609. <https://doi.org/10.1007/s12650-015-0273-2>
- Wang J, Shan R, Zhang C, Feng L (2010) Experimental investigation of a novel two-dimensional synthetic jet. *Eur J Mech B Fluids* 29:342–350. <https://doi.org/10.1016/j.euromechflu.2010.05>
- Wang L, Feng LH, Wang JJ, Li T (2017) Parameter influence on the evolution of low-aspect ratio rectangular synthetic jets. *J vis* 21:105. <https://doi.org/10.1007/s12650-017-0440-8>
- Xia Q, Zhong S (2013) Liquids mixing enhanced by multiple synthetic jet pairs at low Reynolds numbers. *Chem Eng Sci* 102:10–23. <https://doi.org/10.1016/j.ces.2013.07.019>
- Yang AS, Ro JJ, Yang MT, Chang WH (2009) Investigation of piezoelectrically generated synthetic jet flow. *J vis* 12:9–16. <https://doi.org/10.1007/bf03181938>
- Yang E, Ekmekci A, Sullivan PE (2022) Phase evolution of flow controlled by synthetic jets over NACA 0025 airfoil. *J vis* 25:751–765. <https://doi.org/10.1007/s12650-021-00824-5>
- Youmin Y, Simon TW, Zhang M, Yeom T, North MT, Cui T (2014) Enhancing heat transfer in air-cooled heat sinks using piezoelectrically-driven agitators and synthetic jets. *Int J Heat Mass Transf* 68:184–193. <https://doi.org/10.1115/imece2011-6454>
- Zhang D, Yang K, Cheng QH, Gao J (2015) Numerical investigation of heat transfer performance of synthetic jet impingement onto dimpled/protrusioned surface. *Therm Sci* 19(1):221–229. <https://doi.org/10.2298/TSCI15S1S21Z>
- Zhang S, Zhong S (2009) Experimental investigation of flow separation control using an array of synthetic jets. In: 39th AIAA fluid dynamics conference <https://doi.org/10.2514/6.2009-4185>
- Zong H, Kotsonis M (2017) Effect of slotted exit orifice on performance of plasma synthetic jet actuator. *Exp Fluids* 58:17. <https://doi.org/10.1007/s00348-016-2299-1>

**Publisher's Note** Springer Nature remains neutral with regard to jurisdictional claims in published maps and institutional affiliations.

Springer Nature or its licensor (e.g. a society or other partner) holds exclusive rights to this article under a publishing agreement with the author(s) or other rightsholder(s); author self-archiving of the accepted manuscript version of this article is solely governed by the terms of such publishing agreement and applicable law.